A novel model for the lift force acting on a prolate spheroidal particle in an arbitrary non-uniform flow. Part I. Lift force due to the streamwise flow shear

Yan Cui[a,*], Jure Ravnik[b], Matjaž Hriberšek[b], Paul Steinmann[a]

[a] *Chair of Applied Mechanics, Friedrich-Alexander Universität Erlangen-Nürnberg, Paul-Gordan-Str. 3, D-91052 Erlangen, Germany*
[b] *Faculty of Mechanical Engineering, University of Maribor, Smetanova 17, SI-2000, Maribor, Slovenia*

Abstract

The paper proposes a generic method to extend lift force models that were originally devised for single linear shear flow, to arbitrary flow conditions. The method computes the lift force due to the dominant streamwise flow shear in the Stokes flow regime by implementing a series of coordinate transformations, facilitating the computation of the lift force from dominant streamwise flow shear. The derived numerical algorithm is applied to the computation of a dedicated shear lift force model for prolate spheroidal particles (or axisymmetric ellipsoidal particles) and a novel generalised Saffman-type lift force model for spherical particles in a general shear flow. In order to verify the proposed shear lift force for prolate spheroidal particles, numerical simulations of a particle moving in Poiseuille flow at four different initial positions and two aspect ratios are perfomed. The new generalised Saffman-type lift model is compared with an established generalised Saffman-type lift model by simulating the axial migration of a spherical particle in Poiseuille flow. The computational results confirm the correctness of the proposed shear lift force models.

Keywords: prolate spheroidal particle, axisymmetric ellipsoidal particle, shear lift force, Lagrangian particle tracking

*Corresponding author
Email addresses: yan.cui@fau.de (Yan Cui), jure.ravnik@um.si (Jure Ravnik), matjaz.hribersek@um.si (Matjaž Hriberšek), paul.steinmann@fau.de (Paul Steinmann)

1. Introduction

In-depth understanding of fluid flows with dispersed solid particles is important in several fields of sciences, e.g. life sciences, natural sciences, medical sciences and engineering sciences. Processing of suspensions with fibres in the pulp industry (Marchioli et al., 2010), heat transfer augmentation based on the use of particles with favourable thermal properties (Jafari et al., 2008), drug detachment within dry powder inhalers (Cui et al., 2014; Cui & Sommerfeld, 2017), drug deposition in the pulmonary delivery (Koullapis et al., 2017), mixing of particles in stirred tanks (Delafosse et al., 2015), separation of particles in wastewater treatment (Hriberšek et al., 2011) and magnetic separation of particles from liquids (Zadravec et al., 2014) are only a few of many applications.

Dispersed flows consist of particles that interact with the fluid phase, i.e. they exchange mass, linear and angular momentum, and energy. When one derives dedicated numerical methods for the computation of dispersed two-phase flows, the case of small rigid particles travelling in the Stokes flow regime is predominantly taken into account. Furthermore, in the case of dilute suspension of rigid particles, considered in this article, only the fluid flow impact on the particle motion shall be modelled (Crowe et al., 1998). When the particles are smaller than the smallest flow scales, the point source model within the Lagrangian particle tracking framework can be implemented.

As one can not afford to resolve flow structures in the vicinity of the particles directly, it is necessary to apply the appropriate constitutive models for the interaction between the particles and the fluid flow. Among particle-fluid interactions that predominantly influence the particle trajectory, the linear momentum transfer is typically the most important one. However, in the case of high shear flow fields or rotating particles, especially for non-spherical shaped particles, angular momentum must also be considered. In the linear momentum transfer case, the drag force is the predominant fluid force. Besides, when a particle encounters a high shear flow region, the shear-induced lift forces can

significantly influence the particle trajectory and should not be neglected (Derksen, 2003). Theoretically, there are mainly two directions to develop shear lift force models: one focuses on a simple shear around a particle at low particle Reynolds numbers, while the other considers the inviscid limit of week simple shear around a particle at high particle Reynolds numbers (Daly et al., 2014).

The low Reynolds number regime was initially investigated by Saffman (Saffman, 1965, 1968), who found that a sphere moving through a very viscous liquid with velocity relative to a uniform simple shear experiences a lift force perpendicular to the flow direction. However, Saffman didn't account for the wall interaction and the neutrally buoyant limit (Stone, 2000). McLaughlin (1993) built on Saffman's work by calculating the lift force on a particle in a linear shear flow in the presence of the wall. Miyazaki et al. (1995) calculate the mobility tensor of a sphere moving in a fluid by generalising the simple shear flow to an arbitrary linear shear flow. In the case of non-spherical particles, a lift tensor introduced by Harper & Chang (1968) can be used to model the shear-induced lift for any arbitrarily shaped 3D body in a linear shear flow. In the steady limit, the closed form for the mobility tensor of Miyazaki et al. (1995) becomes similar to the lift tensor of Harper & Chang (1968). However, there appears to be some (reasonably small) numerical discrepancy between the mobility tensor and the lift tensor (Stone, 2000). Later Fan & Ahmadi (1995) used the lift tensor of Harper & Chang (1968) to build the shear-induced lift force model for axisymmetric ellipsoidal particles in a linear shear flow.

When a sphere is placed in a weak shear flow of an inviscid fluid under high particle Reynolds numbers, a lift force is generated by the secondary velocity resulting from advection of vorticity by the irrotational component of the flow around the sphere surface (Auton, 1987; Auton et al., 1988). In the case of non-spherical particles, Zhang et al. (2001) pioneered simulations of the transport and deposition of ellipsoidal particles in turbulent channel flow by using empirical models. Hölzer & Sommerfeld (2009) and Zastawny et al. (2012) use direct numerical simulation (DNS) to calculate the shear lift force on differently shaped single particles with a wide range of flow Reynolds numbers. Likewise,

Ouchene et al. (2016) derive and validate new correlations for the lift coefficient for non-spherical particles by fitting the results extracted from DNS computations of the flow around prolate ellipsoidal particles. The highlight of their work is to provide a complete set of correlations for prolate ellipsoidal particles outside the Stokes regime.

A generic approach used to extend lift force models that were originally devised for linear shear flow to arbitrary flow conditions in the Stokes flow regime is proposed in this work. The idea is based on the assumption that the dominant contribution to the flow-induced lift force arises from the streamwise flow shear. As the streamwise direction locally varies in the fluid flow field, the computation of the lift force caused by the streamwise flow shear needs to be performed in a local coordinate system, which has to be aligned with the streamwise direction at the particle location; therefore a suitable coordinate system rotation has to be applied. Another dedicated coordinate system rotation is needed to establish the conditions where a resultant shear can directly be applied in the shear lift models devised for the linear shear flow. Since this approach is applied to extend the lift model of Harper & Chang (1968) from the linear shear flow to the arbitrary flow condition, prerequisites on using Harper & Chang's lift model are needed as well, e.g. particles moving in the regime of creeping flow (Stokes flow).

The paper is organized as follows. In Section 2, the equations of kinematics and dynamics of prolate spheroidal particles are presented, including the translational and rotational motion of particles. Particular attention is devoted to the derivation of the dedicated lift force model for prolate spheroidal particles due to the streamwise flow shear. To prove the numerical algorithm for calculating the generalised shear lift force is not restricted to prolate spheroids, the original Saffman lift force model, which is applicable for spherical particles in a simple shear flow, is extended to the case of an arbitrary shear flow by applying the same computational method. In Section 3, numerical verification of the new shear lift force model for prolate spheroidal particles in Poiseuille flow is presented. The predictions of the present numerical models for prolate

spheroids on the motion of ellipsoidal fibres in low Reynolds number pipe flow are compared with available numerical results (Tian et al., 2012). Moreover, the new generalised Saffman-type lift force is verified against the established generalised Saffman-type lift force proposed by Crowe et al. (1998) in Poiseuille flow. The paper ends with conclusions.

Notation:. *Tensors* of various order are expressed in bold italic font, i.e. a first-order tensor (vector) and a second-order tensor are denoted by $\boldsymbol{A}$ and $\boldsymbol{B}$, respectively. In a Cartesian coordinate system with base vectors $\boldsymbol{e}_i$ ($i = 1,2,3$) they have the coordinate representation $\boldsymbol{A} = A_i\boldsymbol{e}_i$ and $\boldsymbol{B} = B_{ij}\boldsymbol{e}_i \otimes \boldsymbol{e}_j$, respectively, whereby Einstein's summation convention applies for repeated indices. A_i and B_{ij} are the *coefficients* of $\boldsymbol{A}$ and $\boldsymbol{B}$, respectively, in the chosen coordinate system $\boldsymbol{e}_i$. They may be arranged into *coefficient matrices*

$$\boldsymbol{A} := \begin{bmatrix} A_1 \\ A_2 \\ A_3 \end{bmatrix} \quad \text{and} \quad \boldsymbol{B} := \begin{bmatrix} B_{11} & B_{12} & B_{13} \\ B_{21} & B_{22} & B_{23} \\ B_{31} & B_{32} & B_{33} \end{bmatrix}$$

whereby bold sloping sans serif font is used for coefficient matrices. Indeed $\boldsymbol{A}$ is a column matrix, the superscript T denotes transposition so that $\boldsymbol{A}^T = [A_1, A_2, A_3]$ (a row matrix). In the sequel we restrict ourselves to the use of Cartesian coordinate systems $\boldsymbol{e}_i$ and $\boldsymbol{e}'_i$ that are related via rotation with rotation matrix $\boldsymbol{V}$ (or likewise by rotation tensor $\boldsymbol{Q}$), i.e.

$$\boldsymbol{e}'_i = V_{ik}\boldsymbol{e}_k = [V_{lk}\boldsymbol{e}_k \otimes \boldsymbol{e}_l] \cdot \boldsymbol{e}_i =: \boldsymbol{Q} \cdot \boldsymbol{e}_i \quad \text{with} \quad \boldsymbol{Q} = \boldsymbol{V}^T.$$

Without loss of generality we will thus only use the corresponding matrix arrangements of tensor coefficients, i.e. the coefficient matrices

$$\boldsymbol{A}' = \boldsymbol{V}\,\boldsymbol{A} \quad \text{and} \quad \boldsymbol{B}' = \boldsymbol{V}\,\boldsymbol{B}\,\boldsymbol{V}^T.$$

Finally, it is noted that we will use x_1, x_2, x_3 and x, y, z interchangeably.

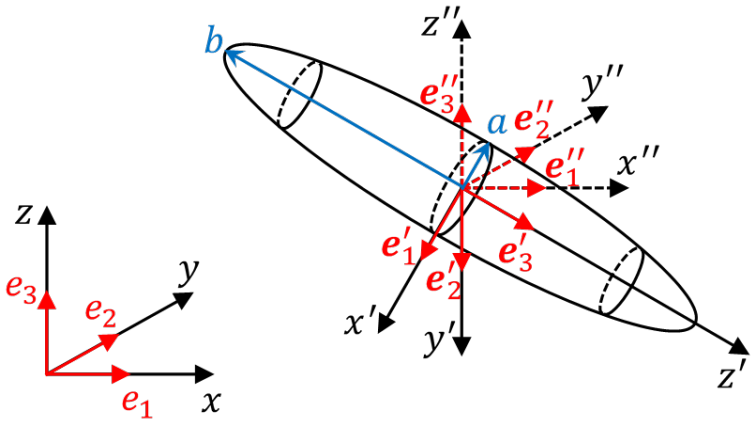

Figure 1: Schematic of a prolate spheroidal particle and the corresponding coordinate system.

2. Equation of Motion for Prolate Spheroidal Particles

2.1. Kinematics

A schematic diagram of a prolate spheroidal particle (or axisymmetric ellipsoidal particle) with semi-minor axis a and semi-major axis b, and thus with aspect ratio $\lambda = b/a \geq 1$, and the associated reference frames are illustrated in Fig. 1. The co-translational frame (or the co-moving frame) $[x'', y'', z'']$ is attached to the prolate spheroidal particle with its origin at the particle centroid and its axes being parallel to the inertial frame $[x, y, z]$. The co-rotational frame (or the particle frame) $[x', y', z']$ is defined with its origin at the centroid of the particle and its axes being along the principal axes of the prolate spheroidal particle, in which z' is in the direction of the semi-major axis.

For tensor coefficients that do not change between the inertial and the co-moving frame (the coefficients of the position vector are an exception) we shall not distinguish between the corresponding coefficient matrices and will thus abstain from the double prime notation in the following sections.

Orientation in space may be parametrised by the Euler angles $[\phi, \theta, \psi]$ by using the x-convention (Goldstein, 1980). However, when kinematic relations between the angles and angular velocity are set up, we observe that a singu-

larity exists for $\theta = 0$ and $\theta = \pi$ (Fantoni, 2008). To avoid this problem, we express the rotation matrix in terms of the Euler parameters (or the quaternions) $[e_0, e_1, e_2, e_3]$, which can be obtained as follows (Goldstein, 1980)

$$\begin{aligned} e_0 &= \cos\left[\frac{1}{2}[\phi+\psi]\right]\cos\left[\frac{\theta}{2}\right], \quad e_1 = \cos\left[\frac{1}{2}[\phi-\psi]\right]\sin\left[\frac{\theta}{2}\right] \\ e_2 &= \sin\left[\frac{1}{2}[\phi-\psi]\right]\sin\left[\frac{\theta}{2}\right], \quad e_3 = \sin\left[\frac{1}{2}[\phi+\psi]\right]\cos\left[\frac{\theta}{2}\right] \end{aligned} \tag{1}$$

The Euler parameters are subject to the constraint $e_0^2 + e_1^2 + e_2^2 + e_3^2 = 1$ (Goldstein, 1980).

The rotation matrix written in terms of the Euler parameters reads in the inertial frame as

$$\boldsymbol{V} = \begin{bmatrix} e_0^2+e_1^2-e_2^2-e_3^2 & 2[e_1e_2+e_0e_3] & 2[e_1e_3-e_0e_2] \\ 2[e_1e_2-e_0e_3] & e_0^2-e_1^2+e_2^2-e_3^2 & 2[e_2e_3+e_0e_1] \\ 2[e_1e_3+e_0e_2] & 2[e_2e_3-e_0e_1] & e_0^2-e_1^2-e_2^2+e_3^2 \end{bmatrix} \tag{2}$$

In the rotational part of the kinematics, the time evolution of the Euler parameters is related to the angular velocity in the vector basis attached to the particle, $\omega_{i'}$ (with $i' = x'$, y', z'), and is given by

$$\begin{aligned} \frac{de_0}{dt} &= \frac{1}{2}[-e_1\omega_{x'} - e_2\omega_{y'} - e_3\omega_{z'}], \quad \frac{de_1}{dt} = \frac{1}{2}[\ e_0\omega_{x'} - e_3\omega_{y'} + e_2\omega_{z'}] \\ \frac{de_2}{dt} &= \frac{1}{2}[\ e_3\omega_{x'} + e_0\omega_{y'} - e_1\omega_{z'}], \quad \frac{de_3}{dt} = \frac{1}{2}[-e_2\omega_{x'} + e_1\omega_{y'} + e_0\omega_{z'}] \end{aligned} \tag{3}$$

2.2. Dynamics of translational motion

The trajectory of a particle is a result of its interaction with the fluid flow. In the case of small particles, typically in the micro and submicron range, the particles behave like rigid bodies, i.e. the deformation of a particle can be neglected. Local values of velocity, vorticity and pressure in the fluid phase and their difference to the state of the particle determine transport phenomena between the dispersed and the fluid phase. Particle transport is computed in the

Euler-Lagrangian framework by particle tracking, which is performed by solving the following ordinary differential equation along the particle trajectories:

$$m_p \frac{d\boldsymbol{v}}{dt} = \boldsymbol{F}_D + \boldsymbol{F}_{SL} + \boldsymbol{g} V_p \left[\rho_p - \rho_f\right] \tag{4}$$

where m_p, V_p, ρ_p are the mass, the volume and the density, respectively, of the particle, ρ_f is the fluid density, and $\boldsymbol{v}$, $\boldsymbol{F}_D$, $\boldsymbol{F}_{SL}$, $\boldsymbol{g}$ are the corresponding coefficient (column) matrices of the particle velocity $\boldsymbol{v}$, the drag force $\boldsymbol{F}_D$, the shear lift force $\boldsymbol{F}_{SL}$, and the gravity acceleration $\boldsymbol{g}$, respectively. The gravity force reduced by buoyancy is captured by the last term in Eq. 4. In the present study, the particle dimensions have a scale of *micrometres* for reasons that will be explained in Section 2.2.2, and the relative velocity (or the slip velocity) between the particle and the fluid is very small, this resulting in a *Stokes flow* around the particle, i.e. particle Reynolds number $Re_p = D_p \left|\boldsymbol{u} - \boldsymbol{v}\right| / \nu \ll 1$, where ν, D_p are the kinematic fluid viscosity and the volume equivalent diameter of the particle, respectively, and $\boldsymbol{u}$ denotes the coefficient (column) matrix of the flow velocity $\boldsymbol{u}$ at the particle's position. Therefore, the profile lift force, the lift force due to the relative particle rotation with respect to the fluid, the Brownian motion force, the pressure gradient force, the added mass, and the Basset history force are neglected (Hjelmfelt & Mockros, 1966; Sommerfeld et al., 2008; Tu et al., 2013).

2.2.1. Drag force

Brenner (1964) derived the hydrodynamic drag force acting on an axisymmetric ellipsoidal particle with semi-minor axis a in the Stokes flow regime:

$$\boldsymbol{F}_D = \pi a \rho_f \nu \boldsymbol{K} \left[\boldsymbol{u} - \boldsymbol{v}\right] =: \boldsymbol{D} \left[\boldsymbol{u} - \boldsymbol{v}\right] \tag{5}$$

Particular to the hydrodynamic drag force in Eq. 5 is the introduction of the (geometric) resistance tensor $\boldsymbol{K}$ with coefficient matrix $\boldsymbol{K}$ (where $\boldsymbol{D} = \pi a \rho_f \nu \boldsymbol{K}$ could be denoted the coefficient matrix of the physical resistance tensor for axisymmetric ellipsoidal particles). In the particle frame of reference $[x', y', z']$

only diagonal components of $\boldsymbol{K'}$ are non-zero, these are a function of the particle aspect ratio λ and may be written as

$$K'_{x'x'} = K'_{y'y'} = \frac{16[\lambda^2 - 1]^{3/2}}{[2\lambda^2 - 3]\ln(\lambda + \sqrt{\lambda^2 - 1}) + \lambda\sqrt{\lambda^2 - 1}} \tag{6}$$

$$K'_{z'z'} = \frac{8[\lambda^2 - 1]^{3/2}}{[2\lambda^2 - 1]\ln(\lambda + \sqrt{\lambda^2 - 1}) - \lambda\sqrt{\lambda^2 - 1}} \tag{7}$$

The spherical particle limit renders $\lim_{\lambda \to 1} \boldsymbol{K'} = 6\,\boldsymbol{I}$, where $\boldsymbol{I}$ is the identity matrix.

To express the coefficients of the resistance tensor in the inertial frame of reference, the rotation matrix $\boldsymbol{V}$ is used:

$$\boldsymbol{K} = \boldsymbol{V}^T\,\boldsymbol{K'}\,\boldsymbol{V}, \tag{8}$$

where $\boldsymbol{K}$ and $\boldsymbol{K'}$ denote the coefficients matrices of the resistance tensor $\boldsymbol{K}$ in the inertial and the particle frame of reference.

2.2.2. Lift force acting on prolate spheroidal particles in a linear shear flow

Harper & Chang (1968) derived a shear lift force model for arbitrarily shaped three-dimensional (3D) rigid bodies moving in a linear shear flow $\boldsymbol{u} = [u_x(z),\, 0,\, 0]$ in the x–z plane (whereby $u_{x,z} = \partial u_x/\partial z$ is constant) in the Stokes flow regime as

$$\boldsymbol{F}_{SL} = \frac{1}{\rho_f\,\nu^{3/2}}\,\frac{u_{x,z}}{|u_{x,z}|^{1/2}}\,\boldsymbol{D}\,\boldsymbol{L}_{xz}\,\boldsymbol{D}\,[\boldsymbol{u} - \boldsymbol{v}] \tag{9}$$

where $\boldsymbol{D}$ is the coefficient matrix of the physical resistance tensor $\boldsymbol{D}$ for arbitrarily shaped 3D rigid bodies. Thereby the coefficient matrix of the lift tensor $\boldsymbol{L}_{xz}$ as calculated via asymptotic methods by Harper & Chang (1968) is expressed as

$$\boldsymbol{L}_{xz} = \begin{bmatrix} A & 0 & B \\ 0 & C & 0 \\ D & 0 & E \end{bmatrix} \tag{10}$$

where the coefficients of $\boldsymbol{L}_{xz}$ are given as

$$A = 0.0501,\; B = 0.0329,\; C = 0.0373,\; D = 0.0182,\; E = 0.0173. \tag{11}$$

Recall that $\boldsymbol{D}$ reads in the case of prolate spheroidal particles as $\boldsymbol{D} = \pi a \rho_f \nu \boldsymbol{K}$, thus one can rewrite the shear lift force of Harper & Chang (1968) as

$$\boldsymbol{F}_{SL} = \pi^2 \rho_f a^2 \sqrt{\nu} \, \frac{u_{x,z}}{|u_{x,z}|^{1/2}} \, \boldsymbol{K} \, \boldsymbol{L}_{xz} \, \boldsymbol{K} \, [\boldsymbol{u} - \boldsymbol{v}] \tag{12}$$

For the limiting case of a spherical particle with $\lim_{\lambda \to 1} \boldsymbol{K} = 6 \, \boldsymbol{I}$ Eq. 12 degenerates to

$$\boldsymbol{F}_{SL} = 36\pi^2 \rho_f a^2 \sqrt{\nu} \, \frac{u_{x,z}}{|u_{x,z}|^{1/2}} \, \boldsymbol{L}_{xz} \, [\boldsymbol{u} - \boldsymbol{v}] \tag{13}$$

If the off-diagonal coefficients D and B are set to zero, the remaining coefficients A, C and E have the effect of changing the shape of the Stokes orbit (Harper & Chang, 1968), and represent the inertial effect of the Stokes drag. For example, coefficient A acts in the x-direction as a result of relative velocity in the x-direction which behaves the same as the x-component of the Stokes drag. The particle motion remains periodic when the off-diagonal coefficients are zero, and the non-zero off-diagonal coefficients render the aperiodic motion of the particle orbit. The coefficient D has a stronger influence on the shear lift force than the coefficient B. This is because the coefficient B acts in the x-direction as a result of relative velocity in the z-direction, while the coefficient D acts in the z-direction and is due to the relative velocity in the x-direction (Harper & Chang, 1968). The z-component lift force induced by the velocity difference in the x-direction agrees with the result of Saffman (Eq. 26), i.e. $36\pi^2 D = 6.46$, which corresponds to the finding of Harper & Chang (1968) and Fan & Ahmadi (1995).

In principle, the lift tensor $\boldsymbol{L}_{xz}$ can be applied to any arbitrarily shaped 3D body (Harper & Chang, 1968) in the Stokes flow regime. It is used to determine the shear lift force for a prolate spheroidal particle by applying the product $\boldsymbol{K} \, \boldsymbol{L}_{xz} \, \boldsymbol{K}$, where the orientation of the prolate spheroid is taken into account by Eq. 8. Therefore, the shear lift force in Eq. 12 is applicable for particles with prolate spheroidal and fibre shapes as well as spherical shape at very low particle Reynolds numbers (i.e. $Re_p \ll 1$) in a linear shear flow.

It should be noted that Harper & Chang (1968) only proposed a general form of the lift force acting on arbitrarily shaped 3D body in a linear shear

flow. The lift model for prolate spheroidal particles was first introduced by Fan & Ahmadi (1995) in a different linear shear flow $\boldsymbol{u} = [u_x(y), 0, 0]$ in the x–y plane (whereby $u_{x,y} = \partial u_x/\partial y$ is constant), which reads as

$$\boldsymbol{F}_{SL} = \pi^2 \rho_f a^2 \sqrt{\nu}\, \frac{u_{x,y}}{|u_{x,y}|^{1/2}}\, \boldsymbol{K}\, \boldsymbol{L}_{xy}\, \boldsymbol{K}\, [\boldsymbol{u} - \boldsymbol{v}] \tag{14}$$

where the coefficient matrix $\boldsymbol{L}_{xy}$ of the lift tensor $\boldsymbol{L}_{xy}$ is a permuted version of $\boldsymbol{L}_{xz}$ and is given by

$$\boldsymbol{L}_{xy} = \begin{bmatrix} A & B & 0 \\ D & E & 0 \\ 0 & 0 & C \end{bmatrix} \tag{15}$$

Note that the main lift force contribution, due to the relative velocity in the x–direction, is now in the y direction.

2.2.3. Lift force acting on prolate spheroidal particles due to the streamwise flow shear

The above models for the shear lift force acting on prolate spheroidal particles are only applicable for linear shear flows. In the following, we propose a new lift force model for arbitrary shear flows, which focuses on the action of the lift force only in the plane perpendicular to the streamwise flow direction at the particle's position. As was also mentioned in the paper of Fan & Ahmadi (1995): "only the lift force due to the streamwise flow shear which is dominant is included in the analysis". The same conclusion can also be made from the works of Saffman (1965, 1968); Harper & Chang (1968); Stone (2000). It is necessary to perform dedicated transformations of the coordinate systems in such a way, that the lift force, induced by the streamwise flow shear, could be determined from Eq. 12. As will be shown, the procedure is based on performing rotation of the coordinate system twice in order to transform a general streamwise shear flow into a linear shear flow. A preliminary study can be found in Ravnik et al. (2013) and Cui et al. (2018).

In a general flow, there exists six shear rates in the non-diagonal components ($i \neq j$) of the velocity gradient tensor $\boldsymbol{G} := \nabla \boldsymbol{u}$ with coefficients $\partial u_i/\partial x_j$

arranged in the coefficient matrix

$$\boldsymbol{G} = \begin{bmatrix} \frac{\partial u_x}{\partial x} & \frac{\partial u_x}{\partial y} & \frac{\partial u_x}{\partial z} \\ \frac{\partial u_y}{\partial x} & \frac{\partial u_y}{\partial y} & \frac{\partial u_y}{\partial z} \\ \frac{\partial u_z}{\partial x} & \frac{\partial u_z}{\partial y} & \frac{\partial u_z}{\partial z} \end{bmatrix} \tag{16}$$

In the case of a pure shear flow, only one non-diagonal component of $\boldsymbol{G}$ is non-zero, and all the diagonal components of $\boldsymbol{G}$ must be equal to zero.

The first coordinate rotation, described by the rotation matrix $\boldsymbol{V}^*$, rotates the inertial frame with base vectors $\boldsymbol{e}_i$ $(i = 1, 2, 3)$ into a new reference frame with base vectors $\boldsymbol{e}_i^*$ $(i = 1, 2, 3)$, so that the $\boldsymbol{e}_1^*$ is parallel to the streamwise direction at the particle location. Therefore, the coefficient (column) matrix of the flow velocity in the coordinate system $\boldsymbol{e}_i$, i.e. $\boldsymbol{u} = [u_x, u_y, u_z]^T$, is transformed into the coefficient (column) matrix of the flow velocity in the coordinate system $\boldsymbol{e}_i^*$, i.e. $\boldsymbol{u}^* = [u_x^*, 0, 0]^T$ with $u_x^* = |\boldsymbol{u}|$, by the rotation matrix $\boldsymbol{V}^*$:

$$\boldsymbol{u}^* = \boldsymbol{V}^* \, \boldsymbol{u} \tag{17}$$

For the efficient construction of the rotation matrix to rotate one vector into another the method by Möller & Hughes (1999) was used in this work.

Since the fluid velocity at the particle location is taken to be tangential to $\boldsymbol{e}_1^*$, the basis $\boldsymbol{e}_i^*$ which corresponds to the Serret-Frenet frame is actually a curvilinear basis except if the component G_{11}^* is zero. In such a basis, the components of $\boldsymbol{G}^*$ cannot be obtained by using a simple rotation matrix because the local vectors do depend on the spatial coordinates and their own spatial derivations matter in the determination of the components of the velocity gradient. To solve this problem we make an assumption:

Assumption 1.

> The spatial rate of change of the fluid velocity at the particle location is approximately zero in the streamwise direction.

In the case of the developed flow the above assumption holds exactly, whereas it also holds when the particle characteristic time scale is much less then the time

scale of the smallest flow structures, i.e. the particle Stokes number is much less than one. The spherical particle Stokes number is defined as

$$St = \frac{2}{9}\frac{\rho_p}{\rho_f}\frac{a^2}{\nu}\frac{u_0}{L}, \tag{18}$$

where u_0 and L are the characteristic fluid velocity scale and the characteristic problem length scale, respectively. To accomadate this condition the maximum particle Stokes number should be less than $\mathcal{O}(10^{-2})$, since the particle trajectories for $St = 0.01$ are close enough to flow streamlines and hence the assumption of small streamwise velocity changes is correct.

Under such a condition, $G^*_{11} = \partial u^*_x/\partial x^* \approx 0$. Therefore, the coefficient matrix of the velocity gradient tensor in the coordinate system $\boldsymbol{e}^*_i$ can be obtained from the rotation of the coefficient matrix of the velocity gradient tensor in the coordinate system $\boldsymbol{e}_i$,

$$\boldsymbol{G}^* = \boldsymbol{V}^* \, \boldsymbol{G} \, \boldsymbol{V}^{*T} \tag{19}$$

As only the lift force due to the streamwise flow shear is included in the analysis, for the flow velocity at the coordinate system $\boldsymbol{e}^*_i$, only two shear rates of $\partial u^*_x/\partial y^*$ and $\partial u^*_x/\partial z^*$ remain to be taken into account. The part of $\boldsymbol{G}^*$, that is taken into account for the computation of the lift force from the streamwise flow shear, in the coordinate system $\boldsymbol{e}^*_i$, is in the form of

$$\boldsymbol{G}^*_{SL} = \begin{bmatrix} 0 & G^*_{12} & G^*_{13} \\ 0 & 0 & 0 \\ 0 & 0 & 0 \end{bmatrix} \tag{20}$$

where $G^*_{12} = \partial u^*_x/\partial y^*$ and $G^*_{13} = \partial u^*_x/\partial z^*$.

As shown in Fig. 2, the second coordinate rotation by the rotation matrix $\boldsymbol{V}^{**}$ is a rotation around the x^*-axis. The goal of the rotation is to align the unit vector $\boldsymbol{e}^{**}_3$ with the direction vector $\boldsymbol{g}^*_{sl}$, where $\boldsymbol{g}^*_{sl} = [0, G^*_{12}, G^*_{13}]^T$ denotes the coefficient (column) matrix of $\boldsymbol{g}^*_{sl}$. In this way, the two shear rates, i.e. G^*_{12} and G^*_{13} in the coordinate system $\boldsymbol{e}^*_i$, are compressed into one shear rate G^{**}_{13} in the new reference frame with base vectors $\boldsymbol{e}^{**}_i$ $(i = 1, 2, 3)$. In other words, the rotation around the x^*-axis by the rotation matrix $\boldsymbol{V}^{**}$ must meet the following

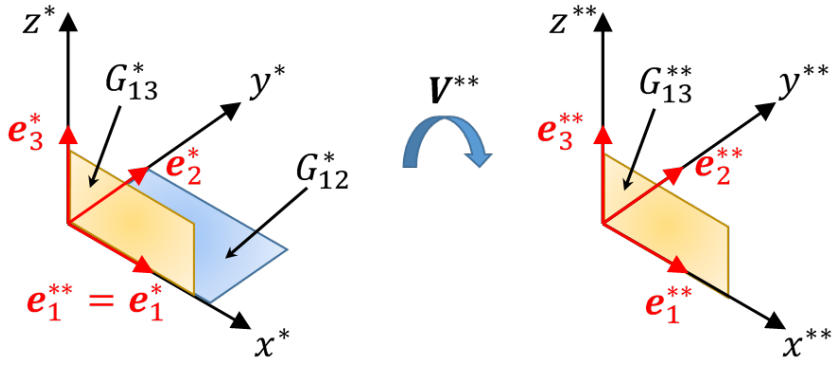

Figure 2: Illustration of the secondary rotation: compose two shear rates into one shear rate by the rotation matrix $\boldsymbol{V}^{**}$.

condition:

$$\boldsymbol{G}_{SL}^{**} = \boldsymbol{V}^{**}\,\boldsymbol{G}_{SL}^{*}\,\boldsymbol{V}^{**T} = \begin{bmatrix} 0 & 0 & G_{13}^{**} \\ 0 & 0 & 0 \\ 0 & 0 & 0 \end{bmatrix} \tag{21}$$

where $G_{13}^{**} = \partial u_x^{**}/\partial z^{**}$. The rotation matrix $\boldsymbol{V}^{**}$ can be calculated by

$$\boldsymbol{e}_3^{**} = \boldsymbol{V}^{**}\,\frac{\boldsymbol{g}_{sl}^{*}}{|\boldsymbol{g}_{sl}^{*}|} \tag{22}$$

where $\boldsymbol{e}_3^{**} = [0, 0, 1]^T$.

After these two rotations, the coefficient matrix of the resistance tensor in the new coordinate system $\boldsymbol{e}_i^{**}$ is given by

$$\boldsymbol{K}^{**} = \boldsymbol{V}^{**}\,\boldsymbol{K}^{*}\,\boldsymbol{V}^{**T} \tag{23}$$

with $\boldsymbol{K}^{*} = \boldsymbol{V}^{*}\,\boldsymbol{K}\,\boldsymbol{V}^{*T}$.

Next, to be able to apply the single linear shear flow model (Harper & Chang, 1968) in a more general case, we propose the following form of the lift force acting on a prolate spheroidal particle in a general shear flow:

$$\boldsymbol{F}_{SL} = \pi^2 \rho_f a^2 \sqrt{\nu}\,\boldsymbol{I} \tag{24}$$

with the coefficient (column) matrix of the lift vector $\boldsymbol{l}$ defined as

$$\boldsymbol{I} = \sqrt{|\boldsymbol{g}_{sl}^{*}|}\,\boldsymbol{V}^{*T}\,\boldsymbol{V}^{**T}\,\boldsymbol{K}^{**}\,\boldsymbol{L}_{xz}\,\boldsymbol{K}^{**}\,\boldsymbol{V}^{**}\,\boldsymbol{V}^{*}\,[\boldsymbol{u} - \boldsymbol{v}] \tag{25}$$

The algorithm for calculating the shear lift force acting on a prolate spheroidal particle from the streamwise flow shear can now be summarised as follows:

Algorithm 1.

1. Compute the rotation matrix $\boldsymbol{V}^*$ by using Eq. 17;
2. Compute the velocity gradient tensor $\boldsymbol{G}^*$ by using Eq. 19;
3. Compute the rotation matrix $\boldsymbol{V}^{**}$ by using Eq. 22;
4. Compute the shear lift force $\boldsymbol{F}_{SL}$ by using Eqs. 23 - 25.

As aforementioned, the lift tensor proposed by Harper & Chang (1968) is applicable for any arbitrarily shaped 3D body. Therefore, *Algorithm 1* can be used to compute the shear lift force on other shaped particles by replacing the (geometric) resistance tensor $\boldsymbol{K}$ for axisymmetric ellipsoids with corresponding (geometric) resistance tensors.

2.2.4. New generalised Saffman-type lift force acting on spherical particles

The proposed algorithm for calculating the lift force from the streamwise flow shear is not restricted to prolate spheroidal particles. It is a generic method that can be used with models that were originally derived under assumptions of single linear shear flow conditions, in order to extend them to arbitrary flow conditions.

In the following, as the single linear shear flow based Saffman lift force model is the most important shear lift model used in numerous particle tracking algorithms, an implementation of the derived algorithm for the Saffman lift is presented.

First, we rewrite the Saffman lift force model for a freely rotating spherical particle moving at a constant velocity in a linear shear flow $\boldsymbol{u} = [u_x(y), 0, 0]$ in the x–y plane (whereby $u_{x,y} = \partial u_x/\partial y$ is constant) at low Reynolds number (Saffman, 1965, 1968) in a 3D form:

$$\boldsymbol{F}_{SL} = 6.46\rho_f a^2 \sqrt{\nu}\, \frac{u_{x,y}}{|u_{x,y}|^{1/2}}\, \boldsymbol{B}\,[\boldsymbol{u} - \boldsymbol{v}] \tag{26}$$

with

$$\boldsymbol{B} = \begin{bmatrix} 0 & 0 & 0 \\ 1 & 0 & 0 \\ 0 & 0 & 0 \end{bmatrix} \tag{27}$$

In the linear shear flow $\boldsymbol{u} = [u_x(y), 0, 0]$, by applying the coefficient matrix $\boldsymbol{B}$ the Saffman lift force points in the y-direction.

Second, a new generalised Saffman-type lift force model is built as follows:

Algorithm 2.

1. Compute the rotation matrix $\boldsymbol{V}^*$ by using Eq. 17;
2. Compute the velocity gradient tensor $\boldsymbol{G}^*$ by using Eq. 19;
3. Compute the rotation matrix $\boldsymbol{V}^{**}$ by using Eq. 22;
4. Compute the new generalised Saffman-type lift force as

$$\boldsymbol{F}_{SL} = 6.46\rho_f a^2\sqrt{\nu}\sqrt{|\boldsymbol{g}^*_{sl}|}\,\boldsymbol{V}^{*T}\,\boldsymbol{V}^{**T}\,\boldsymbol{B}\,\boldsymbol{V}^{**}\,\boldsymbol{V}^{*}\,[\boldsymbol{u}-\boldsymbol{v}] \tag{28}$$

The only difference between *Algorithm 1* and *Algorithm 2* lies in the fourth step, where the coordinate transformations are applied to the sphere (Saffman) lift model instead for the prolate spheroid. Therefore, in the case of a given shear lift model, developed under assumptions of a single linear shear flow, one can build a generalised shear lift force by following the steps (i) to (iv) of *Algorithm 2.*

In Section 3.3, the new generalised Saffman-type lift force is verified against the established generalised Saffman-type lift force proposed by Crowe et al. (1998), expressed here in tensor (vector) notation as

$$\boldsymbol{F}_{SL} = 6.46\rho_f a^2\sqrt{\nu}\frac{1}{\sqrt{|\boldsymbol{w}|}}\,[[\boldsymbol{u}-\boldsymbol{v}]\times\boldsymbol{w}] \tag{29}$$

where $\boldsymbol{w} := \mathrm{curl}\boldsymbol{u}$ is the fluid vorticity (curl of the fluid velocity) on the particle location. In a linear shear flow, the lift component perpendicular to the flow direction calculated by the new generalised Saffman-type lift model (Eq. 28) and the established Saffman-type lift model (Eq. 29) are identical.

2.3. Dynamics of rotational motion

The rotational motion of a non-spherical particle moving in a flow field is governed by

$$I_{x'}\frac{d\omega_{x'}}{dt} - \omega_{y'}\omega_{z'}[I_{y'} - I_{z'}] = T_{x'} \tag{30}$$

$$I_{y'}\frac{d\omega_{y'}}{dt} - \omega_{z'}\omega_{x'}[I_{z'} - I_{x'}] = T_{y'} \tag{31}$$

$$I_{z'}\frac{d\omega_{z'}}{dt} - \omega_{x'}\omega_{y'}[I_{x'} - I_{y'}] = T_{z'} \tag{32}$$

where $\omega_{x'}$, $\omega_{y'}$, $\omega_{z'}$ are the particle angular velocities with respect to the principal axes, $I_{x'}$, $I_{y'}$, $I_{z'}$ are the particle moments of inertia about the principal axes $[x', y', z']$, i.e. the principal values of the particle's inertia tensor, and $T_{x'}$, $T_{y'}$, $T_{z'}$ are the hydrodynamic torques acting on the particle with respect to the principal axes. The rotational motion of the particle in Eqs. (30) - (32) is stated in the particle frame of reference.

The moments of inertia for a prolate spheroid are

$$I_{x'} = I_{y'} = \frac{[1+\lambda^2]a^2}{5}m_p = \frac{4\pi}{15}\lambda[\lambda^2+1]a^5\rho_p \tag{33}$$

$$I_{z'} = \frac{2a^2}{5}m_p = \frac{8\pi}{15}\lambda a^5\rho_p \tag{34}$$

As the flow near a small particle may be approximated as a linear shear flow, Jeffery (1922) derived the hydrodynamic torque acting on a prolate spheroidal particle suspended in a linear shear flow. In the particle frame of reference, we have:

$$T_{x'} = \frac{16\pi\rho_f\nu a^3\lambda}{3[\beta_0+\lambda^2\gamma_0]}\left[[1-\lambda^2]f' + [1+\lambda^2][\xi' - \omega_{x'}]\right] \tag{35}$$

$$T_{y'} = \frac{16\pi\rho_f\nu a^3\lambda}{3[\alpha_0+\lambda^2\gamma_0]}\left[[\lambda^2-1]g' + [1+\lambda^2][\eta' - \omega_{y'}]\right] \tag{36}$$

$$T_{z'} = \frac{32\pi\rho_f\nu a^3\lambda}{3[\alpha_0+\beta_0]}[\chi' - \omega_{z'}] \tag{37}$$

where f', g' are elements of the deformation rate tensor $\boldsymbol{D} := \boldsymbol{G}^{sym}$ and ξ', η' and χ' are elements of the spin tensor $\boldsymbol{W} := \boldsymbol{G}^{skw}$ with $\boldsymbol{w}$ the axial vector of $\boldsymbol{W}$, defined as

$$f' = \frac{1}{2}\left[\frac{\partial u_{z'}}{\partial y'} + \frac{\partial u_{y'}}{\partial z'}\right], \qquad g' = \frac{1}{2}\left[\frac{\partial u_{x'}}{\partial z'} + \frac{\partial u_{z'}}{\partial x'}\right] \tag{38}$$

$$\xi' = \frac{1}{2}\left[\frac{\partial u_{z'}}{\partial y'} - \frac{\partial u_{y'}}{\partial z'}\right], \quad \eta' = \frac{1}{2}\left[\frac{\partial u_{x'}}{\partial z'} - \frac{\partial u_{z'}}{\partial x'}\right], \quad \chi' = \frac{1}{2}\left[\frac{\partial u_{x'}}{\partial y'} - \frac{\partial u_{y'}}{\partial x'}\right] \tag{39}$$

In order to evaluate these terms, the coefficient matrix of the velocity gradient tensor must be rotated into the particle frame of reference using the rotation matrix as

$$\boldsymbol{G'} = \boldsymbol{V}\,\boldsymbol{G}\,\boldsymbol{V}^T \tag{40}$$

The nondimensional coefficients α_0, β_0 and γ_0 were defined by Gallily & Cohen (1979) as

$$\alpha_0 = \beta_0 = \frac{\lambda^2}{\lambda^2 - 1} + \frac{\lambda}{2[\lambda^2 - 1]^{3/2}} \ln\left(\frac{\lambda - \sqrt{\lambda^2 - 1}}{\lambda + \sqrt{\lambda^2 - 1}}\right) \tag{41}$$

$$\lambda^2\gamma_0 = -\frac{2\lambda^2}{\lambda^2 - 1} - \frac{\lambda^3}{[\lambda^2 - 1]^{3/2}} \ln\left(\frac{\lambda - \sqrt{\lambda^2 - 1}}{\lambda + \sqrt{\lambda^2 - 1}}\right) \tag{42}$$

Inserting moments of inertia (33) - (34) and torques (35) - (37) into the equations of motion (30) - (32) and the governing equations for the rotational motion of prolate spheroidal particles are obtained:

$$\frac{d\omega_{x'}}{dt} = \omega_{y'}\omega_{z'}\frac{\lambda^2 - 1}{1 + \lambda^2} + \frac{20\nu}{a^2[\beta_0 + \lambda^2\gamma_0]}\frac{\rho_f}{\rho_p}\left[\frac{1 - \lambda^2}{1 + \lambda^2}f' + [\xi' - \omega_{x'}]\right] \tag{43}$$

$$\frac{d\omega_{y'}}{dt} = \omega_{z'}\omega_{x'}\frac{1 - \lambda^2}{1 + \lambda^2} + \frac{20\nu}{a^2[\alpha_0 + \lambda^2\gamma_0]}\frac{\rho_f}{\rho_p}\left[\frac{\lambda^2 - 1}{1 + \lambda^2}g' + [\eta' - \omega_{y'}]\right] \tag{44}$$

$$\frac{d\omega_{z'}}{dt} = \frac{20\nu}{a^2[\alpha_0 + \beta_0]}\frac{\rho_f}{\rho_p}[\chi' - \omega_{z'}] \tag{45}$$

A MATLAB program used for simulating the motion of prolate spheroidal particles in a 3D flow was developed by using the above models. The implicit Euler backward scheme was applied in the code.

3. Numerical Verification

3.1. Numerical verification of the novel shear lift force model for prolate spheroidal particles

The novel shear lift force model for prolate spheroidal particles is verified in Poiseuille flow as shown in Fig. 3. As the pipe is placed vertically this means

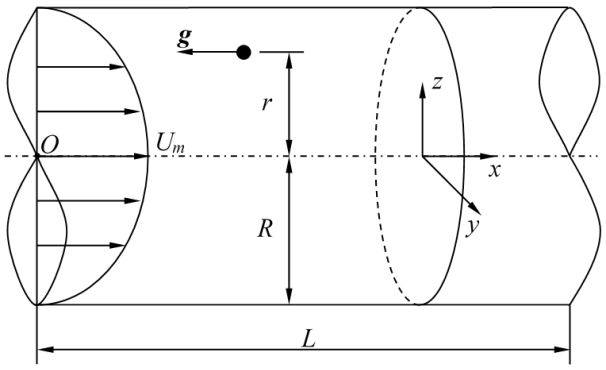

Figure 3: Schematic diagram of a particle in Poiseuille flow with the flow in the x-direction.

the gravity acceleration $\boldsymbol{g}$ is in the $-x$-direction. The gravity can help increase the particle slip velocity, and thus increases the lift force. The pipe radius R is 2.1 mm. The fluid is water with density of $1000\,kg/m^3$ and kinematic viscosity of $1\,mm^2/s$. The velocity profile of the Poiseuille pipe flow is analytically given in cylindrical coordinates ($r = 0$ denoting the centreline of the pipe) by the expression

$$u = U_m \left[1 - \left[\frac{r}{R}\right]^2\right] \tag{46}$$

where U_m is the maximum flow velocity at $r = 0$, with its value set to $0.5\,m/s$ in the present study. In the numerical simulation, only a single particle is placed in the fluid domain with its primary axis b pointing in the direction of the pipe centreline. The volume equivalent diameter of the particle $D_p = 20\,\mu m$, and its density is $2560\,kg/m^3$. The initial vertical distance between the particle and the centreline of the pipe is $r = 0.1\,mm$. The initial velocity of the particle is set to $\boldsymbol{v} = 0.99\,\boldsymbol{u}$, therefore the particle Reynolds number at the starting point is about 0.1. Due to the velocity gradients in the radial direction, the shear lift force is produced and due to its action, the particle is moved to the centreline of the pipe. Regardless of the initial circumferential location of the particle, at the same distance r, a particle must experience the same magnitude of the shear lift force, which has to act radially towards the centre of the pipe.

As aforementioned, the above numerical models have several restrictions.

Point	Position	Euler Angle	Flow Direction
P_1	$[0, -r, 0]^T$	$[0, \pi/2, 0]^T$	$[0.5U_m, 0, 0]^T$
P_2	$[0, -0.866r, 0.5r]^T$	$[0, \pi/3, 0]^T$	$[0.5U_m, 0, 0]^T$

Table 1: Information of two points P_1 and P_2 located in the y-z plane of a Poiseuille flow with the flow in the x-direction.

First, in a Stokes flow the particle Reynolds number must be much less than one. Secondly, the torque obtained by Jeffery (1922) is valid when the inertia of the fluid does not affect the angular motion, i.e. in the limit where the shear Reynolds number, $Re_g = D_p^2 G/\nu$, is zero. Moreover, the validity of *Assumption 1* can be checked by calculating the ratio between G_{11}^{**} and G_{13}^{**}, which must be close to zero. Therefore, we run a test simulation by placing a spherical particle on the y-axis (information on the location of the particle is summarised in Table 1 as P_1) and track the particle for $50\,s$. The time evolution of above dimensionless parameters are illustrated in Fig. 4, and it's obvious that the above three requirements are satisfied in the present simulation.

To verify the developed shear lift model, we first placed the particle at two different positions in the y–z plane with the same radial distance r, with information on the location of the two points summarised in Table 1. P_1 is located on the y-axis so that the shear lift model by Fan & Ahmadi (1995) (Eq. 14) can be directly applied. Fig. 5 plots the translational motion of the particle for different aspect ratios and initial positions. In the case of a spherical particle, the particle moves straight towards the pipe centreline; in the case of a prolate spheroidal particle, the particle moves to the pipe centreline as well, but its trajectory is a periodic curve, caused by the action of the torque resistance. At the position P_1, the results of the present shear lift model show excellent agreement with Fan and Ahmadi's model for both aspect ratios. When moving the particle from position P_1 to P_2, the application of *Algorithm 1* is necessary in order to apply the streamwise shear lift model, and the corresponding computational results prove that there are no differences in the computed particle trajectory.

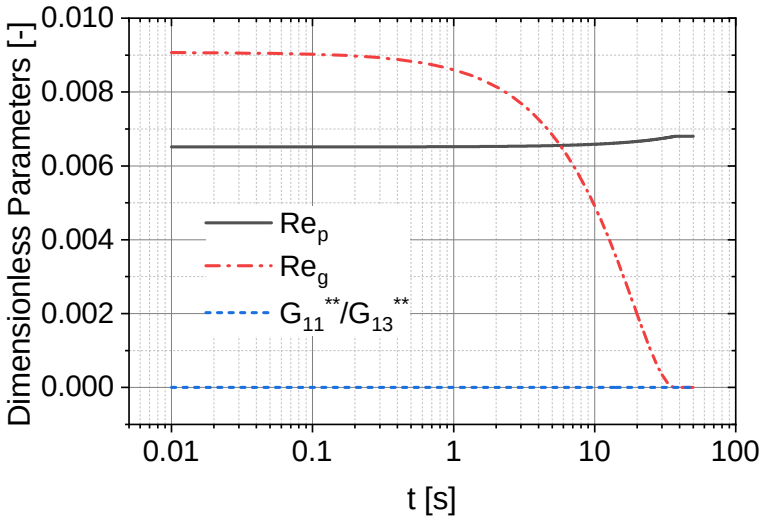

Figure 4: Time evolution of dimensionless parameters of the spherical particle in Poiseuille flow (tracking time: $50\,s$, time step: $10\,\mu s$).

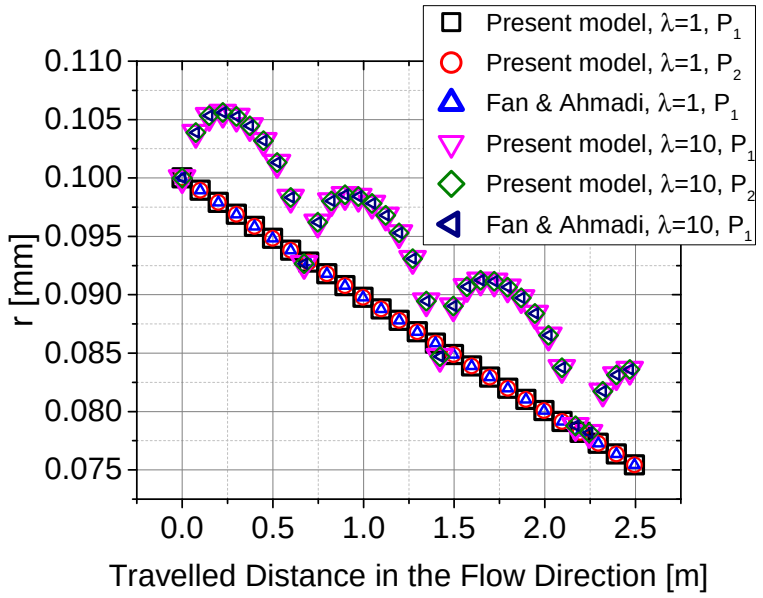

Figure 5: The translational motion of prolate spheroidal particles for different aspect ratios and initial positions (tracking time: $5\,s$, time step: $10\,\mu s$).

Point	Position	Euler Angle	Flow Direction
P_3	$[0.7071r, -0.7071r, 0]^T$	$[\pi/4, \pi/2, 0]^T$	$[U_m/\sqrt{2}, U_m/\sqrt{2}, 0]^T$
P_4	$[0.6124r, -0.6124r, 0.5r]^T$	$[\pi/4, \pi/3, 0]^T$	$[U_m/\sqrt{2}, U_m/\sqrt{2}, 0]^T$

Table 2: Information of two points P_3 and P_4 located in a Poiseuille flow with the flow in the $[U_m/\sqrt{2}, U_m/\sqrt{2}, 0]$ direction.

However, the above results only demonstrate that the coordinate transformation by $\boldsymbol{V}^{**}$ is correct, but the transformation by $\boldsymbol{V}^{*}$ is not verified since due to the verification setup it was an identity matrix. To test both $\boldsymbol{V}^{*}$ and $\boldsymbol{V}^{**}$, the pipe is rotated around the z-axis counterclockwise by the angle of $\pi/4$, resulting in a new flow direction of $[U_m/\sqrt{2}, U_m/\sqrt{2}, 0]^T$, and the gravity acceleration $\boldsymbol{g}$ is switched to the reverse flow direction. After the modification in the flow setup, the previous position of P_1 has become P_3, and P_2 is transformed into P_4, with the information on the location of two new points summarised in Table 2. The particle trajectories of all three different initial particle locations, i.e. P_1, P_3 and P_4, are plotted in Fig. 6. Under the same aspect ratio, i.e. $\lambda = 1$ or 10, the particle trajectories for all three different initial particle locations are identical, proving the validity of the sequential transformations $\boldsymbol{V}^{*}$ and $\boldsymbol{V}^{**}$ for calculating the shear lift force.

3.2. Numerical verification of the transport of ellipsoidal fibres in low Reynolds number pipe flow

The developed Lagrangian particle tracking code is verified by comparing its prediction with avaiable numerical results on the transport and deposition of ellipsoidal fibres in low Reynolds number pipe flow Tian et al. (2012). The same verification case was also used by Feng & Kleinstreuer (2013). The ellipsoidal fibre can be represented by the prolate spheroid at large aspect ratios, e.g. in the present case the aspect ratio $\lambda = 14$. The simulation setup of Tian et al. (2012) is close to the Poiseuille flow case as shown in Fig. 3 with several minor changes. The semi-minor axis of the prolate spheroid is $a = 0.5\,\mu m$. The initial position

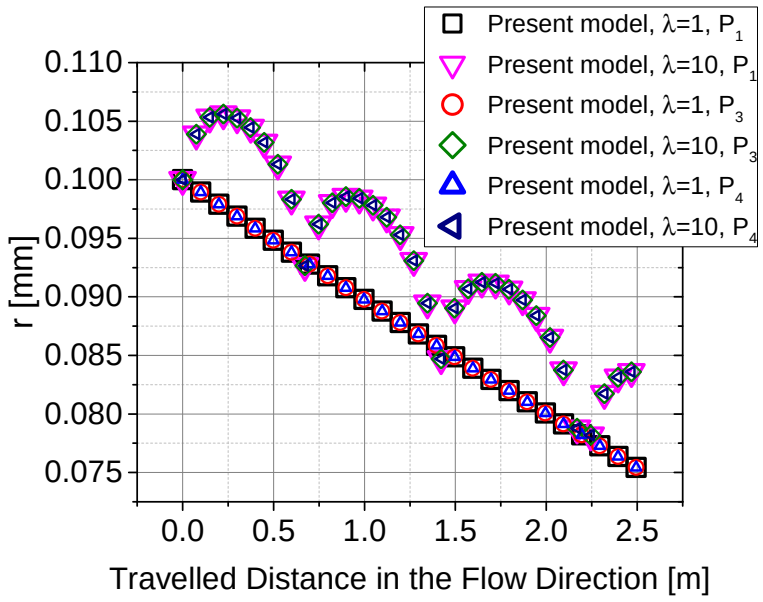

Figure 6: Translational motion of prolate spheroidal particles for different aspect ratios and initial positions (tracking time: $5\,s$, , time step: $10\,\mu s$).

of the particle is $[0, 1.65\,mm, 0]^T$. The initial velocity of the particle is zero, resulting in the flow-driven acceleration of the particle at the beginning. The gravity acceleration is in the $-y$-direction. Based on their flow Reynolds number (i.e. $Re = 169$), the considered fluid is air at 15.62°C, with the corresponding density of $1.208\,kg/m^3$ and the kinematic fluid viscosity of $1.491 \cdot 10^{-5}\,mm^2/s$. The value of $U_m = 0.97\,m/s$ was used as it produces a nice fit with the developed axial velocity profile of Tian et al. (2012). The magnitude of radial velocity in their developed velocity profile are very small and was thus neglected in the present study. As in the original experiment (Tian et al., 2012) the particle was injected in the middle of the pipe length direction, from where the pipe has fully developed flow, the fitting of the axial velocity profile is therefore justified for the verification of the present results.

In Fig. 8 comparison of the orientation of the ellipsoidal fibre between the present numerical results and the results of Tian et al. (2012) in form of the

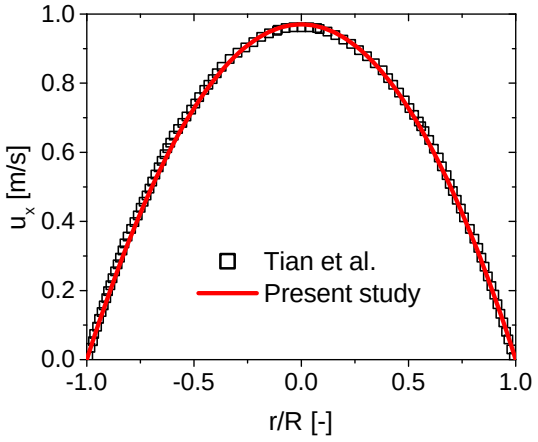

Figure 7: Axial velocity profile at the cross section of the pipe, comparison with the axial velocity profile of Tian et al. (2012).

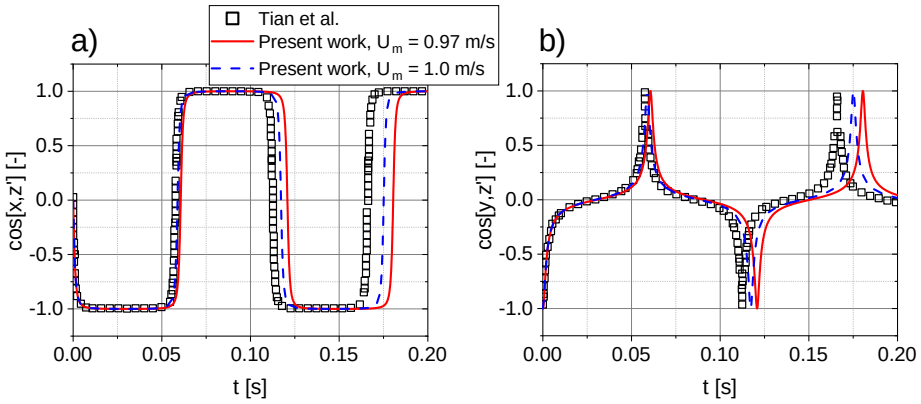

Figure 8: Time evolution of the orientation of an prolate spheroid in the pipe flow ($\lambda = 14$, tracking time: $0.2\,s$, time step: 0.0001 to $0.02\,\mu s$).

directional cosines of the angles formed by the ellipsoidal primary axis b and the inertia frame during its trajectory path is presented. During the first $0.1\,s$ the present numerical results in the form of the temporal evolvement of the orientation of the ellipsoidal fibre agree very well with results of Tian et al. (2012), while afterwards, the magnitudes and rotational patterns still show good agreement, but the flipping of the particle occurs with a different frequency than the particle of Tian et al. (2012). The reason may lie in the difference in the velocity profile and its gradients between the computed pipe flow of Tian et al. (2012) and the Poiseuille flow. By increasing the maximum flow velocity slightly from $0.97\,m/s$ to $1.0\,m/s$, a phase shift in particle orientation in the results becomes apparent, as shown in Fig. 8. The velocity profile is shown to be a sensitive parameter which can induce an evident frequency mismatch. Moreover, the velocity profile is analytical given in the present study, while the accuracy of velocity profile used by Tian et al. (2012) is mesh-dependent and the developed velocity profile along the pipe may change slightly. The numerical accuracy between velocity profiles can also produce the difference.

The above numerical verification is not an ideal test case for the shear lift force since the gravity acts in the same direction as the lift. The particle has the maximum shear lift force at the beginning of the simulation since the initial velocity of the particle is zero so that the velocity difference between the particle and the fluid is the largest. The flow accelerates the particle, and the shear lift force decreases significantly from $4.9\,pN$ to $0.0017\,pN$ within a short time, i.e. $0.0003\,s$. Afterwards, the velocity difference becomes very small. The x-component of the shear lift force is between $0.0012\,pN$ and $0.0019\,pN$ which range is slightly larger than the range of the y-component of the shear lift force, i.e. $0.0005\,pN$ - $0.0012\,pN$. This is reasonable since the inertial effect of the Stokes drag produced by the coefficient A is larger than the lift force generated by the coefficient D.

In order to produce a test case with a more pronounced action of the shear lift force, the setting of the P_1 as described in Section 3.1 is used again. Now the gravity acceleration vector points to the $-x$-direction, hence the translational

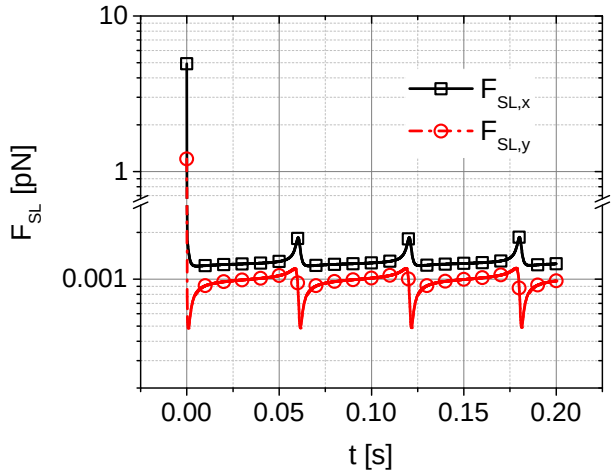

Figure 9: Time evolution of the shear lift force acting on the prolate spheroid ($\lambda = 14$, tracking time: $0.2\,s$, time step: 0.0001 to $0.02\,\mu s$).

movement of the particle in the radial direction is dominated by the shear lift force. As the present lift model is not only valid for prolate spheroids and fibres but also valid for spherical particles, it is possible to compare the new lift model with the generalised Saffman-type lift force proposed by Crowe et al. (1998) (Eq. 29). Fig. 10 plots the particle trajectories for different numerical models and aspect ratios. In the case of spherical particle, the particle trajectories of the present shear lift model (Eq. 24) and the generalised Saffman-type lift model show an excellent agreement. In the case of prolate spheroidal particle, the particle rotates due to the flow resistance, and this rotation brings a change in the direction of the resulting fluid force, i.e. $\boldsymbol{F}_D + \boldsymbol{F}_{SL}$. As a result, the particle trajectory becomes a periodic curve and approaches to the centreline of the pipe. When increasing the aspect ratio from 1 to 10, the period of the rotational motion grows. Fig. 11 shows the orientation of the prolate spheroidal particle. Eventually, the absolute value of $\cos[x, z']$ becomes one and $\cos[y, z']$ reaches zero, meaning the primary axis b of the prolate spheroidal particle is oriented into the flow direction, where the particle with this orientation angle experiences a minimum drag with also the velocity gradient at the centreline of

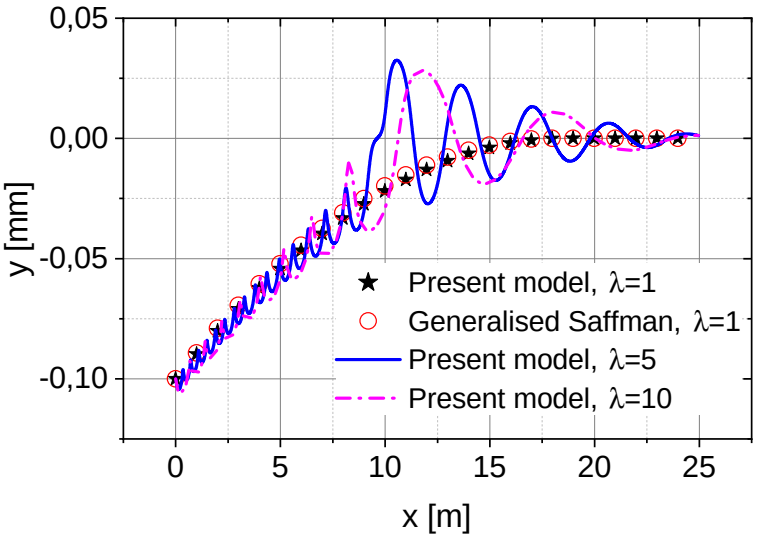

Figure 10: The translational motion of a prolate spheroidal particle in Poiseuille flow (tracking time: $50\,s$, time step: $10\,\mu s$).

the pipe being zero.

3.3. Numerical verification of the new generalised Saffman-type lift model

To verify the new generalised Saffman-type lift model as described in *Algorithm 2*, the same simulation setup as described in Section 3.1 is applied. Fig. 12 plots the particle trajectories for two different initial positions (i.e. P_1 and P_4) and two generalised Saffman-type lift models (i.e. the current approach and the Crowe's model). As expected, the results at P_1 and P_4 calculated by the same lift models are identical. Moreover, the results between the two models show an excellent agreement, proving the validity of the sequential transformations $\boldsymbol{V}^*$ and $\boldsymbol{V}^{**}$ for extending the use of the shear lift models that were originally devised for a single linear shear flow, to arbitrary flow conditions.

4. Conclusions

In the present paper, a novel shear lift force model for prolate spheroidal particles (or axisymmetric ellipsoidal particles) that can be used for Lagrangian

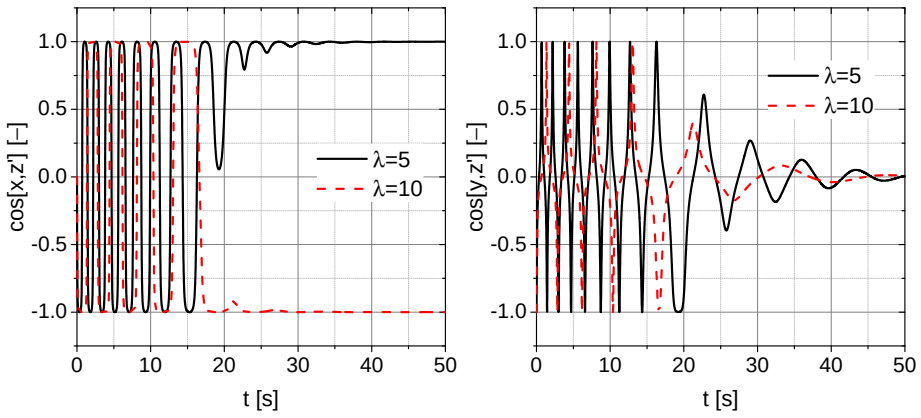

Figure 11: The orientation of a prolate spheroidal particle in Poiseuille flow (tracking time: $50\,s$, time step: $10\,\mu s$).

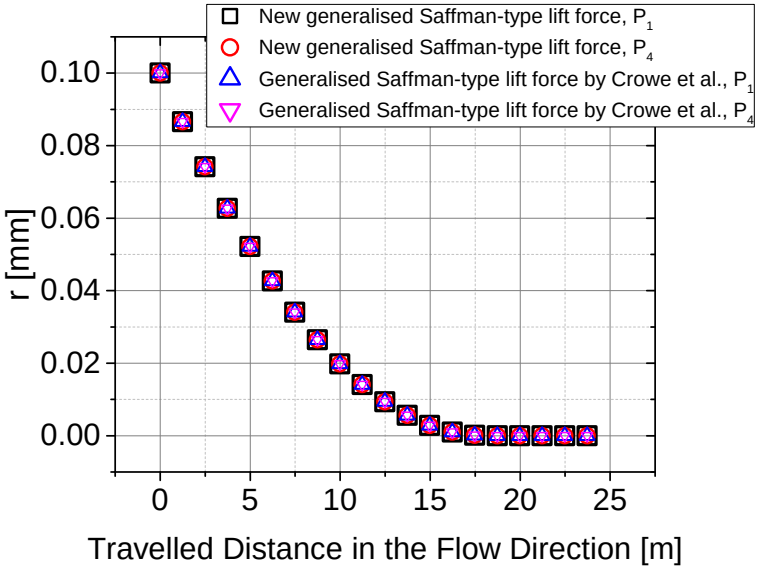

Figure 12: The translational motion of a spherical particle in Poiseuille flow for two different generalised Saffman-type lift models (tracking time: $50\,s$, time step: $10\,\mu s$).

particle tracking is presented. The primary objective of the present study is the evaluation of the drag force and the shear flow induced lift force with respect to the orientation of prolate spheroidal particles. Instead of the Euler angles parametrisation of the rotation matrix in Euler parameters/quaternions are used to avoid singularity issues. The time evolution of the Euler parameters is related to the angular velocity of the prolate spheroidal particle, resulting from rotational dynamics, whereas as the resistance to the rotational motion the linear Jeffery torque (Jeffery, 1922) is adopted. To account for the effect of the particle shape in the Stokes flow regime the resistance tensor of Brenner (1963) is implemented. The main contribution of the present paper lies in the derivation of a computational algorithm for the evaluation of the shear-induced lift force, acting on a prolate spheroidal particle. The approach of Harper & Chang (1968) based on the lift tensor and the single linear shear flow is used as the starting point. By considering that the dominant contribution to the shear lift force is the streamwise flow shear, a double rotation of the frame of reference, in which the shear lift force is evaluated, is developed. The first rotation is used for transformation into a local coordinate system, aligned with the streamwise direction at the particle location. The second rotation is used for subsequent transformation, ensuring that a general streamwise shear flow is mapped into a linear shear flow, for which the model of Harper & Chang (1968) can be applied. Moreover, this sequential coordinate transformations is not restricted to compute the shear lift force acting on prolate spheroidal particles, and also allows the extension of the use of the shear lift models that were originally devised for a single linear shear flow, to arbitrary flow conditions. As an example, a new generalised Saffman-type lift force model is derived by following the same procedures.

The new computational algorithm for the evaluation of the shear lift force acting on prolate spheroidal particles is verified in Poiseuille pipe flow. By placing the particle at different circumferential positions in the pipe and by keeping the radial direction constant the computed particle trajectories for four different initial positions and two different aspect ratios are identical, proving the

exactness of the developed rotational transformations. The predictions of the present numerical models for prolate spheroids on the motion of ellipsoidal fibres in low Reynolds number pipe flow are compared with available numerical results (Tian et al., 2012). The obtained numerical results of the temporal evolution of the orientation of the ellipsoidal fibre agree very well with Tian et al. (2012) for the starting phase of the particle-fluid interaction, while afterwards, the flipping of the particle occurs with a different frequency than the particle of Tian et al. (2012). The reason mainly lie in the difference in the velocity profile and its gradients between the computed pipe flow of Tian et al. (2012) and the Poiseuille flow. The new generalised Saffman-type lift force model is verified against the established generalised Saffman-type lift model proposed by Crowe et al. (1998) in Poiseuille flow. The excellent agreement between the results of two different lift models proves the ability of extensive application of the present algorithm.

In some special cases, e.g. lid-driven cavity flow, the non-streamwise flow shear (or the cross-stream shear) also plays an important role on the lift and shall not be neglected. In the companion paper, referred as Part II, the lift force due to the non-streamwise flow shear will be taken into account. The improved model in the companion paper is less accurate than the present model in fluid flows which are dominated by streamwise shear but can be applied to a broader range of applications.

Acknowledgement: the authors thank the Deutsche Forschungsgemeinschaft for the financial support in the framework of the project STE 544/58.

Declarations of interest: none.

References

Auton, T. R. (1987). The lift force on a spherical body in a rotational flow. *Journal of Fluid Mechanics*, *183*, 199. doi:10.1017/s002211208700260x.

Auton, T. R., Hunt, J. C. R., & PrudHomme, M. (1988). The force exerted on a body in inviscid unsteady non-uniform rotational flow. *Journal of Fluid Mechanics*, *197*, 241. doi:10.1017/s0022112088003246.

Brenner, H. (1963). The Stokes resistance of an arbitrary particle. *Chem. Eng. Sci*, *18*, 1–25.

Brenner, H. (1964). The Stokes resistance of an arbitrary particle - IV. Arbitrary fields of flow. *Chem. Eng. Sci*, *19*, 703–727.

Crowe, C. T., Sommerfeld, M., & Tsuji, Y. (1998). *Multiphase flows with droplets and particles*. CRC press.

Cui, Y., Ravnik, J., Hriberšek, M., & Steinmann, P. (2018). On constitutive models for the momentum transfer to particles in fluid-dominated two-phase flows. In *Advanced Structured Materials* (pp. 1–25). Springer International Publishing. doi:10.1007/978-3-319-70563-7_1.

Cui, Y., Schmalfuß, S., Zellnitz, S., Sommerfeld, M., & Urbanetz, N. (2014). Towards the optimisation and adaptation of dry powder inhalers. *International Journal of Pharmaceutics*, *470*, 120–132.

Cui, Y., & Sommerfeld, M. (2017). Application of lattice-boltzmann method for analysing detachment of micron-sized particles from carrier particles in turbulent flows. *Flow, Turbulence and Combustion*, .

Daly, T., Pannala, S., & Ruggles, A. (2014). *Integrated lift- and wall-force closures in CMFD*. Technical Report University of Tennessee-Knoxville, Oak Ridge National Laboratory.

Delafosse, A., Calvo, S., Collignon, M.-L., Delvigne, F., Crine, M., & DominiqueToye (2015). Eulerï£¡lagrange approach to model heterogeneities instirred tank bioreactors ï£¡ comparison to experimental flow characterization and particle tracking. *Chemical Engineering Science*, (p. 457ï£¡466).

Derksen, J. J. (2003). Numerical Simulation of Solids Suspension in a Stirred Tank. *AIChE Journal*, *49*, 2700–2714.

Fan, F., & Ahmadi, G. (1995). A sublayer model for wall deposition of ellipsoidal particles in turbulent streams. *J. Aerosol Sci.*, *26*, 813–840.

Fantoni, M. (2008). *Dynamics of ellipsiodal particles dispersed in channel flow turbulence*. Ph.D. thesis University of Udine.

Feng, Y., & Kleinstreuer, C. (2013). Analysis of non-spherical particle transport in complex internal shear flows. *Physics of Fluids*, *25*.

Gallily, I., & Cohen, A.-H. (1979). On the orderly nature of the motion of nonspherical aerosol particles II. Inertial collision between a spherical large droplet and axially symmetrical elongated particle. *J. Colloid Interface Sci.*, *68*, 338–356.

Goldstein, H. (1980). *Classical Mechanics, 2nd Edition*. Addison Wesely, Reading MA.

Harper, E. Y., & Chang, I. D. (1968). Maximum dissipation resulting from lift in a slow viscous shear flow. *J. Fluid Mech.*, *33*, 209–225.

Hjelmfelt, A. T., & Mockros, L. F. (1966). Motion of discrete particles in a turbulent fluid. *Applied Scientific Research*, *16*, 149–161. doi:10.1007/bf00384062.

Hölzer, A., & Sommerfeld, M. (2009). Lattice boltzmann simulations to determine drag, lift and torque acting on non-spherical particles. *Computers & Fluids*, *38*, 572–589. doi:10.1016/j.compfluid.2008.06.001.

Hriberšek, M., Žajdela, B., Hribernik, A., & Zadravec, M. (2011). Experimental and numerical investigations of sedimentation of porous wastewater sludge flocs. *Water Research*, *45*, 1729–1735. doi:10.1016/j.watres.2010.11.019.

Jafari, A., Tynjälä, T., Mousavi, S. M., & Sarkomaa, P. (2008). Simulation of heat transfer in a ferrofluid using computational fluid dynamics technique. *International Journal of Heat and Fluid Flow*, *29*, 1197–1202.

Jeffery, G. B. (1922). The motion of ellipsoidal particles immersed in a viscous fluid. *Proc. R. Soc. A*, *102*, 161–179.

Koullapis, P., Kassinos, S., Muela, J., Perez-Segarra, C., Rigola, J., Lehmkuhl, O., Cui, Y., Sommerfeld, M., Elcner, J., Jicha, M., Saveljic, I., Filipovic, N., Lizal, F., & Nicolaou, L. (2017). Regional aerosol deposition in the human airways: The SimInhale benchmark case and a critical assessment of in silico methods. *European Journal of Pharmaceutical Sciences*, .

Marchioli, C., Fantoni, M., & Soldati, A. (2010). Orientation, distribution and deposition of elongated, inertial fibers in turbulent channel flow. *Phys. Fluids*, *49*, 33301.

McLaughlin, J. B. (1993). The lift on a small sphere in wall-bounded linear shear flows. *Journal of Fluid Mechanics*, *246*, 249. doi:10.1017/s0022112093000114.

Miyazaki, K., Bedeaux, D., & Avalos, J. B. (1995). Drag on a sphere in slow shear flow. *Journal of Fluid Mechanics*, *296*, 373. doi:10.1017/s0022112095002163.

Möller, T., & Hughes, J. F. (1999). Efficiently building a matrix to rotate one vector to another. *Journal of Graphics Tools*, *4*, 1–4.

Ouchene, R., Khalij, M., Arcen, B., & Tanière, A. (2016). A new set of correlations of drag, lift and torque coefficients for non-spherical particles and large reynolds numbers. *Powder Technology*, *303*, 33–43. doi:10.1016/j.powtec.2016.07.067.

Ravnik, J., Marchioli, C., Hriberšek, M., & Soldati, A. (2013). On shear lift force modelling for non-spherical particles in turbulent flows. In G. P. T. E. Simos, & C. Tsitouras (Eds.), *AIP*

Conference Proceedings (pp. 1107–1110). Rhodes, Greece volume 1558. URL: http://scitation.aip.org/content/aip/proceeding/aipcp/10.1063/1.4825700http://dx.doi.org/10.1063/1.4825700. doi:10.1063/1.4825700.

Saffman, P. G. (1965). The lift on a small sphere in a slow shear flow. *J. Fluid Mech.*, *22*, 385.

Saffman, P. G. (1968). Corrigendum to: The lift on a small sphere in a slow shear flow. *J. Fluid Mech.*, *31*, 624.

Sommerfeld, M., van Wachem, B., & Oliemans, R. (2008). *Best Practice Guidelines for Computational Fluid Dynamics of Dispersed Multi-Phase Flows*. ERCOFTAC.

Stone, H. A. (2000). Philip Saffman and viscous flow theory. *J. Fluid Mech.*, *409*, 165–183.

Tian, L., Ahmadi, G., Wang, Z., & Hopke, P. K. (2012). Transport and deposition of ellipsoidal fibers in low Reynolds number flows. *Journal of Aerosol Science*, *45*, 1–18.

Tu, J., Inthavong, K., & Ahmadi, G. (2013). *Computational Fluid and Particle Dynamics in the Human Respiratory System*. Springer Netherlands. doi:10.1007/978-94-007-4488-2.

Zadravec, M., Hriberšek, M., Steinmann, P., & Ravnik, J. (2014). High gradient magnetic particle separation in a channel with bifurcations. *Engineering Analysis with Boundary Elements*, *49*, 22–30. URL: http://dx.doi.org/10.1016/j.enganabound.2014.04.012http://www.sciencedirect.com/science/article/pii/S0955799714000897. doi:http://dx.doi.org/10.1016/j.enganabound.2014.04.012.

Zastawny, M., Mallouppas, G., Zhao, F., & van Wachem, B. (2012). Derivation of drag and lift force and torque coefficients for non-spherical particles in flows. *Int. J. Multiphase Flow*, *39*, 227–239.

Zhang, H., Ahmadi, G., Fan, F. G., & McLaughlin, J. B. (2001). Ellipsoidal particles transport and deposition in turbulent channel flows. *Int. J. Multiphase Flow*, *27*, 971–1009.